Title: Numerical prediction of diffusion and electric field-induced iron nanoparticle transport

Author: Helena I. Gomes José Miguel Rodríguez-Maroto Alexandra B. Ribeiro Sibel Pamukcu Celia Dias-Ferreira

PII: S0013-4686(14)02387-1
DOI: http://dx.doi.org/doi:10.1016/j.electacta.2014.11.157
Reference: EA 23829

To appear in: *Electrochimica Acta*

Received date: 22-9-2014
Revised date: 23-11-2014
Accepted date: 25-11-2014

Please cite this article as: Helena I.Gomes, José Miguel Rodríguez-Maroto, Alexandra B.Ribeiro, Sibel Pamukcu, Celia Dias-Ferreira, Numerical prediction of diffusion and electric field-induced iron nanoparticle transport, Electrochimica Acta http://dx.doi.org/10.1016/j.electacta.2014.11.157

Numerical prediction of diffusion and electric field-induced iron nanoparticle transport

Helena I. Gomes[a,d], José Miguel Rodríguez-Maroto[b,1], Alexandra B. Ribeiro[a], Sibel Pamukcu[c,1], Celia Dias-Ferreira[d]

[a] CENSE, Departamento de Ciências e Engenharia do Ambiente, Faculdade de Ciências e Tecnologia, Universidade Nova de Lisboa, 2829-516 Caparica, Portugal

[b] Department of Chemical Engineering, University of Málaga, Campus de Teatinos, 29071-Málaga, Spain

[c]Department of Civil and Environmental Engineering, Fritz Engineering Laboratory, 13 E. Packer Avenue, Lehigh University, Bethlehem, PA 18015-4729, USA

[d]CERNAS – Research Center for Natural Resources, Environment and Society, Escola Superior Agraria de Coimbra, Instituto Politecnico de Coimbra, Bencanta, 3045-601 Coimbra, Portugal

* Corresponding author. Tel. +351 212948300, Fax. +351 212948554. E-mail address: hrg@campus.fct.unl.pt (Helena I. Gomes)

[*]Corresponding author. Tel.: +351 212948300; fax.: +351 212948554

[1]ISE member

Highlights

- Numerical model describes the nZVI transport by diffusion and under electric fields
- Data from different porosity media and electrolytes were used to validate the model
- Diffusion, electromigration, electrophoresis and electroosmosis were considered
- Aggregation of nZVI particles due to high suspension concentrations
- Electrophoretic transport of the nZVI is counteracted by electroosmosis

Abstract

Zero valent iron nanoparticles (nZVI) are considered very promising for the remediation of contaminated soils and groundwaters. However, an important issue related to their limited mobility remains unsolved. Direct current can be used to enhance the nanoparticles transport, based on the same principles of electrokinetic remediation. In this work, a generalized physicochemical model was developed and solved numerically to describe the nZVI transport through porous media under electric field, and with different electrolytes (with different ionic strengths). The model consists of the Nernst–Planck coupled system of equations, which accounts for the mass balance of ionic species in a fluid medium,when both the diffusion and electromigration of the ions are considered. The diffusion and electrophoretic transport of the negatively charged nZVI particles were also considered in the system. The contribution of electroosmotic flow to the overall mass transport was included in the model for all cases.The nZVI effective mobility values in the porous medium are very low (10^{-7}-10^{-4} $cm^2V^{-1}s^{-1}$), due to the counterbalance between the positive electroosmotic flow and the electrophoretic transport of the negatively charged nanoparticles. The higher the nZVI concentration is in the matrix, the higher the aggregation; therefore, low concentration of nZVI suspensions must be used for successful field application.

Nomenclature

A cross-sectional area (cm2)

c concentration (mol cm-3)

*D** effective diffusion coefficient

E redox potential (V)

E^0 standard redox potential (V)

F Faraday constant

I current intensity

k_e electroosmotic permeability coefficient

N mass flux (mol cm2 s-1)

Q reaction quotient

R ideal gas constant

R reaction rate

T temperature (K), assuming a constant room temperature of 25ºC

t time

U* effective electrophoretic mobility

V volume (cm3)

z ionic charge

Greek letters

ϕ electrical potential

η Faradaic efficiency

Subscripts

i species

j cell

Keywords: Electrokinetics; nZVI; porous media; electrolytes;Nernst–Planck equations

1. Introduction

Zero valent iron was used successfullyfor soil and groundwater remediation in permeable reactive barriersfor more than two decades[1-3]. With the development of advanced nanotechnologies since late nineties, due to their size and reactivity that allowed an easy injection,zero valent iron nanoparticles (nZVI) were considered a promising step forward in soil and groundwater clean-up, particularly targeting organochlorines [4-8]. The nZVI transport in porous media was studied in column tests with sand [9-16], glass beads [17-19] and model soils [20, 21]. These studies showed that nZVI has a tendency to aggregate quickly and settle in the pores, primarily due to magnetic attractive forces [22]. Results from field scale applications [23-27] confirm this limited mobility, ranging from 1 m [28] to 6-10 m [26], depending on soil characteristics, test operations, and injection velocities [29].

One of the methods tested to overcome poor nZVI mobility was the use of direct current (DC) [16, 30-34], using the same principles of electrokinetic remediation (EKR). In this method, low-level direct current is the “cleaning agent”, inducing different transport mechanisms (electroosmosis, electromigration and electrophoresis) and electrochemical reactions (electrolysis and electrodeposition) in contaminated soils [35]. Direct comparison of the resultsprovided in previous studies on nZVI enhanced transport with direct current is limited due to the differences in experimental setups, soils or other solid media used, types of iron nanoparticles, injection places (i.e., directly in the soil, anode or cathode compartments), magnitude and duration of the voltage gradients applied. In general electrophoretic transport of the particles was shown to be predominant in sandy soil [33, 36, 37], while electro-osmotic transport appeared more important in kaolin clay and loamy sand soil [16, 32]. The available analytical models of the nanoparticle transport in literature include only the electrophoretic effect that mostly takes place in sands [33, 37].

The numerical modeling of electrokinetic remediation of heavy metals contaminated soils was first implemented by Wilson et al [38, 39], and lately adapted also for organic contaminants [40, 41]. Further developments include the electrodialytic and dialytic treatment of a fly ash [42], and also the electrokinetic desalination treatments [43].

In this work, a generalized physicochemical model has been developed to describe the electrically induced transport of nZVI particles through different types of porous media of varying porosity and surface reactivity. The model is sufficiently detailed,including the fundamental processes, and its numerical solution offers a reliable predictionof the nZVI transport. Experimental data using different porosity media and different pore fluid electrolytes were used to validate the model [30, 31].

2. Experimental

2.1. Experimental procedure

The experimental data used for the validation of the model have been published previously by Gomes et al[30, 31], where the experimental conditions are described in detail. The experiments were designed so that the transport of nZVI took place in the domain of a layer of porous solid (kaolin and/or glass beads) saturated with an electrolyte.

The experiments were conducted in a modified electrophoretic cell (Econo-Submarine Gel Unit, model SGE-020) as shown in Figure 1.The cell is a rectangular translucent box 10 cm height, 40 cm long and 23 cm width, with a square (20 cm x 20 cm) sample tray and a lid that covers the whole apparatus. Two liquid chambers hold the anolyte and the catholyte and platinum working electrodes on either side of the sample tray (Figure 1). In all experiments, both the anolyte and catholyte compartments were filled with the same electrolyte solution (volume of 650 mL each, Table 1) as that used to saturate the porous specimen. The level of the solutions in the side compartments was kept slightly below the

specimen surface,thus preventing preferential transport of nZVI through a liquid pool over the specimen. Compressed fiberglass wool pads, saturated and immersed in the electrolyte solution, helped transport the migrating ions from the solution into the specimen and vice versa. Different porosity and surface reactivity test media, ranging from glass beads (with particle diameter less than 1 mm, previously sieved) to white Georgia kaolinite clay (> 2 μm) were used in the transport experiments (Table 1). The polyacrylic acid coated iron nanoparticles (PAA-nZVI) suspensions were freshly prepared before each experiment, according to the method used by Kanel et al [18] and had a concentration of 4 g L^{-1} of nZVI. The particle size distribution of the nanoparticles had a mean particle diameter value of 63 nm and the median size was 60.2 nm, based on a count of 420 particlesin TEM images [30, 31]. Two sets of control experiments were conducted for each mixture under the same conditions, one without direct current but with PAA-nZVI, and another with current but without PAA-nZVI. In the experiments with current, a constant potential was applied for 48 h. The cell was kept in a dark location to prevent iron photo-oxidation. The nanoparticle suspension was delivered in the electrophoretic cell using a syringe to inject 2 mL through a tube, which allowed the suspension disperse into a pre-cut shallow channel in the porous specimen between the auxiliary electrodes E2 and E3.

The soil and aqueous samples were analyzed for total iron and ferrous iron concentrations. The iron was extracted from the test medium with the sodium dithionite-citrate-bicarbonate (DCB) method. The iron analyses were conducted using a Perkin-Elmer AAnalyst 200 flame atomic absorption spectroscopy (AAS) and a Hach DR 2800 spectrophotometer (UV).

2.2. Model description

The analytical model operates in two steps: first the kinetic process is simulated by integrating forward in time the one-dimensional transport equations, including the

electrochemical reactions at the electrodes; then the chemical equilibriums are reestablished before the next step of integration. This is done because chemical equilibriums are considered instantaneous when compared with the transport time.

2.2.1 Governing equations

The mass conservation equation for i^{th} species in a j^{th} volume element, including electrochemical reactions, is described by:

$$V_j\left(\frac{dc_{ij}}{dt}\right) = \left(N_{i,j-1} + N_{i,j}\right)A + R_i V_j \quad (1)$$

where V_j is volume of water in j^{th} cell (cm^3), $c_{ij}$is the concentration of i^{th} species (ions and nZVI) in the aqueous phase of the j^{th} volume element (mol cm^{-3}), t is the time, $N_{i,j-1}$and $N_{i,j}$ the mass flux of i^{th} species from $(j\text{-}1)^{th}$ into j^{th} element volume and from j^{th} into $(j+1)_{th}$volume element (mol cm^2 s^{-1}), A cross-sectional area of the domain (cm^2), and R_i the reaction rate for i species. With respect to the chemical reactions, only the chemical equilibria and the electrochemical reactions at the electrodes are considered.

The model consists of a coupled system of Nernst–Planck equations, which accounts for the mass balance of the ionic species in a fluid medium, when diffusion and electromigration are considered in the transport process. In the case of charged nZVI (i.e., the nanoparticles are stabilized with polyacrylic acid – PAA, which gives them the negative charge), diffusion and electrophoretic terms have to be taken into account. The electroosmotic flow is included in all cases.

Therefore, the flux of any chemical species or charged particles $i$from a j^{th} volume element of the system can be expressed as:

$$N_i = -D_i^* \nabla c_i - U_i^* c_i \nabla \phi - k_e c_i \nabla \phi \quad (2)$$

where (sub index *j* is omitted), c_i is the molar concentration, D_i^* is the effective diffusion coefficient, and $\nabla \phi$ is the electrical potential, $k_e$is the electroosmotic permeability coefficient and U_i^*, is the effective electrophoretic mobility for nZVI charged particles or effective ionic mobility, estimated by the Einstein–Nernst relation for ions [44]:

$$U_i^* = \frac{D_i^* z_i F}{RT} \tag{3}$$

where R is the ideal gas constant, F is the Faraday constant, z_i is the ionic charge of the species and T is the temperature (K), assuming a constant room temperature of 25 ºC.The value of the electroosmotic permeability coefficient usually is in a very tight range of 10^{-5} to 10^{-4} cm^2 s^{-1} V^{-1}[45]. Electroosmotic permeability and mobility can be combined into a new effective mobility in the porous medium, U_i^{**}:

$$U_i^{**} = U_i^* + k_e \tag{4}$$

The mass balance equations for nZVI and the ionic species are integrated over the one-dimensional region limited by the electrodes compartments in order to obtain the concentration profile for a given set of experimental conditions. Due to the negative charge of polyacrylic acid coated nZVI, the sign of electrophoretic term is negative, whereas the electroosmotic term is positive, resulting in a low value for the effective mobility.

Table 1 shows the experimental conditions and parameters used in solution of the model to simulate the experimental tests. The nZVI effective diffusion coefficient values in Table 1 were obtained from fitting the experimental results, that varied between 0.5×10^{-5} and 5.9×10^{-5} cm^2 s^{-1}.The electrophoretic mobility (EPM) of PAA-nZVI was obtained from experimental measures for the different particle suspensions using Laser Doppler Velocimetry in a ZetaSizer Nano ZS, Malvern (Southborough, MA). Stock suspensions of PAA-nZVI were diluted to 2 g L^{-1} to obtain measurements for the electrolytes used in the transport tests.

2.2.3. Electrochemical reactions

The rate of generation term is not included in the continuity equation for the porous specimen because we assume that the main chemical reactions that need to be considered are the electrochemical reduction and oxidation of water at the electrodes. The other electrochemical reactions had to be taken into account only in experiments 10 and 11, as explained in the following paragraphs. Nernst equation is used to calculate the redox potential for each electrochemical half reaction, as:

$$E = E^0 - \frac{RT}{\upsilon F} \ln Q \tag{5}$$

where Q is the reaction quotient, defined as the product of the activities of the chemical species to the power of their stoichiometric coefficients, for non-equilibrium conditions. In the special case that the reaction is at equilibrium, the reaction quotient is equal to the equilibrium constant at 25º C. υ in this case is the stoichiometric coefficient of the electrons in the redox equation, i.e. the number of electrons exchanged during the oxidation or reaction process. E (V) is the redox potential in the reduction sense and E^0 (V) is the standard redox potential, which is measured under standard conditions which are 25 ºC, 1 M concentration for each ion participating in the reaction, a partial pressure of 1 atm is assigned for each gas that is part of the reaction and metals in their pure state [46].

At the cathode, cations Na^+ and Ca^{2+} are attracted, but the redox potential of alkali and alkaline earth metals is too high to be competitive to that of water in aqueous media. Consequently, it seems reasonable to assume that only water reduction is taking place at the cathode. Thus, the only electrochemical half-reaction at the cathode is:

$$2H_2O + 2e^- \rightarrow 2OH^-(aq) + H_2(gas) \qquad E^0 = -0.828 \text{ V} \tag{6}$$

On the other hand, anions are attracted to the anode, where oxidation reactions occur. In the most of experiments (5 to 9 and 12) only water oxidation is expected. In contrast, the

oxidation of ions Cl^- (0.1 M) in experiment 10 and of ions $SO_3^=$ (0.1 M) in experiment 11 could compete with the water oxidation at the anode. Therefore, the possible half-reactions at the anode is given by equation (7) for experiments 5 to 9 and 12; by equations (7) and (8) for experiment 10; and by equations (7) and (9) for experiment 11:

$$2H_2O \rightarrow 4H^+(aq) + O_2(gas) + 4e^- \qquad E^0 = -1.229 \text{ V} \qquad (7)$$

$$2Cl^- \rightleftarrows Cl_2 + 2e^- \qquad E^0 = -1.360 \text{ V} \qquad (8)$$

$$SO_3^= + 2OH^- \rightleftarrows SO_4^= + 2e^- + H_2O \qquad E^0 = 0.936 \text{ V} \qquad (9)$$

Although a slight smell to chlorine was detected in experiment 10, the calculations revealed that even in the most favourable conditions (pH < 1) the fraction of current used for chloride oxidation is negligible. On the contrary, the sulphite oxidation predominates at the anode in the experiment 11.

The electrochemical reactions were included in the mass balance equations of anode and cathode compartments as given in equations (10) and (11) for all the experiments, with the exception of experiment 11 which also included the equations (12) and (13):

$$V_0\left(\frac{dc_{10}}{dt}\right)_{ER} = \frac{I}{F}\eta \qquad (10)$$

$$V_{N+1}\left(\frac{dc_{2N+1}}{dt}\right)_{ER} = \frac{I}{F}\eta \qquad (11)$$

$$V_0\left(\frac{dc_{40}}{dt}\right)_{ER} = -\frac{I}{zF}\eta \qquad (12)$$

$$V_0\left(\frac{dc_{120}}{dt}\right)_{ER} = \frac{I}{zF}\eta \qquad (13)$$

where V_0 and $V_{N+1}$are the volumes of electrolyte in the anodic and cathodic compartments, c_{10} and c_{2N+1}, H^+ and OH^- concentrations generated there by electrochemical reactions, c_{40} and c_{120}, $SO_3^=$ and $SO_4^=$ concentrations at the anodic compartment corresponding to the mass of

sulfite and sulfate consumed and generated by oxidation respectively, I is the current intensity, F, the Faraday's constant and η the Faradic efficiency.

2.2.4. Chemical equilibria

Once the transport calculations are completed at each time step, the value of concentration corresponding to the chemical equilibrium of every species is calculated from the last value obtained from the transport. Therefore, in every volume element a system of non-linear equations given by the mass balances, the electrical neutrality condition, and the equilibrium mass action equations were solved.

The extremely rapid reactions between protons and hydroxyls to form water and reverse must be taken into account in all the experiments. The chemical equilibrium of water is:

$$H^+ + OH^- \rightleftarrows H_2O \qquad K_w = \left[H^+\right]\left[OH^-\right] = 10^{-14} \tag{14}$$

In the experiments using NaCl (0.001 M) as electrolyte, as no equilibrium process affects Cl^- and Na^+, the conservation equations for them are trivial. In contrast, additional equilibrium equations are necessary for the experiments 9, 10 and 11, using NaOH (0.001 M), $CaCl_2$ (0.05 M) and Na_2SO_3 (0.1 M) as electrolytes, respectively. The exchanges between the atmospheric CO_2 and the electrolyte were also considered in the simulations:

$$CO_3^{=} + H^+ \rightleftarrows HCO_3^- \Rightarrow K_1 = \frac{\left[HCO_3^-\right]}{\left[CO_3^{=}\right]\left[H^+\right]} = 2.13 \cdot 10^{10} \tag{15}$$

$$CO_3^{=} + 2H^+ \rightleftarrows H_2CO_3 \Rightarrow K_2 = \frac{\left[H_2CO_3\right]}{\left[CO_3^{=}\right]\left[H^+\right]^2} = 4.8 \cdot 10^{16} \tag{16}$$

$$Na^+ + H_2O - H^+ \rightleftarrows NaOH \Rightarrow K_3 = \frac{\left[NaOH\right]\left[H^+\right]}{\left[Na^+\right]} = 1.27 \cdot 10^{-14} \tag{17}$$

$$CO_3^{=} + Na^+ \rightleftarrows NaCO_3^- \Rightarrow K_4 = \frac{\left[NaCO_3^-\right]}{\left[CO_3^{=}\right]\left[Na^+\right]} = 18.6 \tag{18}$$

The only effect expected of Ca^{2+} ion is its precipitation as $Ca(OH)_2$ due to the high pH present in the cathodic zone.

$$Ca^{2+} + 2OH^- \rightleftarrows Ca(OH)_2 \qquad K_0 = \left[Ca^{2+}\right]\left[OH^-\right]^2 = 5.02\cdot10^{-6} \tag{19}$$

In fact, in this experiment, a white precipitate was observed at the cathode compartment as predicted by the model calculations.

In the case of sulfite, several equilibrium equations were taken into account:

$$SO_3^{=} + H^+ \rightleftarrows HSO_3^- \Rightarrow K_1 = \frac{\left[HSO_3^-\right]}{\left[SO_3^{=}\right]\left[H^+\right]} = 1.55\cdot10^{-7} \tag{20}$$

$$SO_3^{=} + 2H^+ \rightleftarrows H_2SO_3 \Rightarrow K_2 = \frac{\left[H_2SO_3\right]}{\left[SO_3^{=}\right]\left[H^+\right]^2} = 1.1\cdot10^{9} \tag{21}$$

$$Na^+ + H_2O - H^+ \rightleftarrows NaOH \Rightarrow K_3 = \frac{\left[NaOH\right]\left[H^+\right]}{\left[Na^+\right]} = 1.27\cdot10^{-14} \tag{22}$$

$$SO_3^{=} + Na^+ \rightleftarrows NaSO_3^- \Rightarrow K_4 = \frac{\left[NaSO_3^-\right]}{\left[SO_3^{=}\right]\left[Na^+\right]} = 6.76 \tag{23}$$

$$2SO_3^{=} + 2H^+ - H_2O \rightleftarrows S_2O_5^{2-} \Rightarrow K_5 = \frac{\left[S_2O_5^{2-}\right]}{\left[SO_3^{=}\right]^2\left[H^+\right]^2} = 7.41\cdot10^{-15} \tag{24}$$

$$SO_4^{=} + H^+ \rightleftarrows H\,SO_4^- \Rightarrow K_6 = \frac{\left[HSO_4^-\right]}{\left[SO_4^{=}\right]\left[H^+\right]} = 97.72 \tag{25}$$

3. Results and Discussion

The model reproduces satisfactorily the nZVI concentration profiles in the porous media, as well as the anodic and cathodic pH values over time.

Model and experimental results for nZVI concentrations profiles in the variousporous specimens at the end of the 48 h diffusion control tests are presented in Figure 2. It was detected that, in some cases, an important fraction of the nZVI tends to aggregate when the

concentration is high relative to the available pore volume, becoming immobile. In fact, in experiments 2 and 4 only about 19% and 8% of the injected nZVI remained mobile over the experiment, respectively. At high iron nanoparticle concentration (1-6 g L^{-1}) there is higher agglomeration [11]. Also, when iron nanoparticles aggregate they become larger than the pores, restricting their transport through the matrix [47].

Model and experimental results for nZVI concentrations profiles and pH at the anode and cathode over time in enhanced transport tests are presented in Figures 3 and 4. As can be seen, the concentration of nZVI away from the injection point is higher than in the experiments without current, in all the cases.This result shows that the current enhances nZVI transport by preventing or hindering the nZVI aggregation at the injection location. In Figure 5, the mobile mass of nZVI *vs.*pore volume is shown for the nZVI transport without and with current. In all cases, the mobile mass is higher in the experiments with current.

The model predicts very low effective mobility values in the porous medium (U_i^{**}) as showed in Table 1 as a consequence of the opposing transport directions between the electroosmotic advection and the electrophoretic migration of the negatively charged nanoparticles. This effect manifests itself as higher concentrations close to the injection point in most of experiments. Thus, if the nanoparticles could be stabilized with a surface modifier to give them a positive charge, the nZVI effective mobility could potentially be increased.Nevertheless the probability of the positively charged particles be attracted onto the soil particle surfaces, particularly clays, could increase. Also the use of stabilizers without charge could enhance the electroosmotic transport of the iron nanoparticles.

The ionic strength of the electrolyte was also determinant in the transport of the nanoparticles – the higher the ionic strength of the electrolyte the lower the transport, what should also be considered for field applications with contaminated groundwaters with high concentrations of salts and metals. The distance covered by iron nanoparticles when using

0.001 M NaCl as the electrolyte is approximately the double when compared with 0.05 M $CaCl_2$ and 0.1 M Na_2SO_3(Table2).

Figure 6 shows the model predictions of the transport distance covered by the iron nanoparticles using different electrolytes and porous media, with and without current. It is clearly distinct the enhancement of the nZVI transport when current in applied, especially in the kaolin clay. When using only kaolin clay and direct current the predicted distance covered by iron nanoparticles is almost the double of diffusion only.

4. Conclusions

Both the experimental and the model results showed that an important aggregation of nZVI occurs when the nanoparticles are allowed to diffuse into the porous medium from an injection point. The higher the nZVI concentration is in the matrix, the higher the aggregation; therefore, low concentrations nZVI suspensions must be used for successful field application.The use of electrical current to transport the nanoparticles prevents or hinders the nZVI particle aggregation, increasing their mobility. However, opposing directions of electrophoretic transport of negatively charged particles and the electroosmotic advection still produces low nZVI transport. To enhance this transport, possible solutions could be reversing the charge of the iron nanoparticle surface or by using neutrally charged nanoparticles, both of which could be transported by electroosmotic advection.

Acknowledgments

This work has been funded by the research grant SFRH/BD/76070/2011, by project PTDC/AGR-AAM/101643/2008 NanoDC under Portuguese National funds through “Fundação para a Ciência e a Tecnologia” and by FP7-PEOPLE-IRSES-2010-269289-ELECTROACROSS. The Department of Civil and Environmental Engineering at Lehigh University is acknowledged for the funding of equipment development, testing and analysis of the nZVI transport experiments.

References

[1] USEPA, Permeable Reactive Barrier Technologies for Contaminant Remediation, in, Technical Innovation Office. Office of Solid Waste and Emergency Response U. S. Environmental Protection Agency Washington DC, National Risk Management Research Laboratory Office of Research and Development, U. S. Environmental Protection Agency Cincinnati, Ohio 1998.

[2] S. Comba, A. Di Molfetta, R. Sethi, Water Air Soil Poll., 215 (2011) 595-607.

[3] J.M. Rodríguez-Maroto, F. García-Herruzo, A. García-Rubio, C. Gómez-Lahoz, C. Vereda-Alonso, Chemosphere, 74 (2009) 804-809.

[4] C.-B. Wang, W. Zhang, Environ. Sci.Technol., 31 (1997) 2154-2156.

[5] W. Zhang, C.B. Wang, H.L. Lien, Catal.Today, 40 (1998) 387-395.

[6] J. Dries, L. Bastiaens, D. Springael, S.N. Agathos, L. Diels, Environ. Sci.Technol., 39 (2005) 8460-8465.

[7] Y. Liu, H. Choi, D. Dionysiou, G.V. Lowry, Chem.Mater., 17 (2005) 5315-5322.

[8] H. Song, E.R. Carraway, Environ. Sci.Technol., 39 (2005) 6237-6245.

[9] B.W. Hydutsky, E.J. Mack, B.B. Beckerman, J.M. Skluzacek, T.E. Mallouk, Environ. Sci.Technol., 41 (2007) 6418-6424.

[10] S. Kanel, D. Nepal, B. Manning, H. Choi, J. Nanopart. Res., 9 (2007) 725-735.

[11] T. Phenrat, H.-J. Kim, F. Fagerlund, T. Illangasekare, R.D. Tilton, G.V. Lowry, Environ. Sci. Technol., 43 (2009) 5079-5085.

[12] T. Raychoudhury, G. Naja, S. Ghoshal, J. Contam. Hydrol., 118 (2010) 143-151.

[13] T. Raychoudhury, N. Tufenkji, S. Ghoshal, Water Res., 46 (2012) 1735-1744.

[14] T. Raychoudhury, N. Tufenkji, S. Ghoshal, Water Res., 50 (2014) 80-89.

[15] N. Saleh, H.-J. Kim, T. Phenrat, K. Matyjaszewski, R.D. Tilton, G.V. Lowry, Environ. Sci. Technol., 42 (2008) 3349-3355.

[16] G.C.C. Yang, H.C. Tu, C.-H. Hung, Sep.Purif. Technol. 58 (2007) 166-172.

[17] P. Jiemvarangkul, W.X. Zhang, H.L. Lien, Chem. Eng. J., 170 (2011) 482-491.

[18] S.R. Kanel, R.R. Goswami, T.P. Clement, M.O. Barnett, D. Zhao, Environ. Sci.Technol., 42 (2008) 896-900.

[19] Y.H. Lin, H.H. Tseng, M.Y. Wey, M.D. Lin, Sci. Total Environ., 408 (2010) 2260-2267.

[20] F. He, D. Zhao, J. Liu, C.B. Roberts, Ind. Eng. Chem. Res., 46 (2007) 29-34.

[21] B. Schrick, B.W. Hydutsky, J.L. Blough, T.E. Mallouk, Chem.Mater., 16 (2004) 2187–2193.

[22] T. Phenrat, N. Saleh, K. Sirk, R.D. Tilton, G.V. Lowry, Environ. Sci. Technol., 41 (2007) 284-290.

[23] D.W. Elliott, W. Zhang, Environ. Sci.Technol., 35 (2001) 4922-4926.

[24] J. Quinn, C. Geiger, C. Clausen, K. Brooks, C. Coon, S. O'Hara, T. Krug, D. Major, W.-S. Yoon, A. Gavaskar, T. Holdsworth, Environ. Sci.Technol., 39 (2005) 1309-1318.

[25] K.W. Henn, D.W. Waddill, Remediation, 16 (2006) 57-77.

[26] W. Zhang, D.W. Elliott, Remediation, (2006) 7-21.

[27] C. Su, R.W. Puls, T.A. Krug, M.T. Watling, S.K. O'Hara, J.W. Quinn, N.E. Ruiz, Water Res., 46 (2012) 5071-5084.

[28] C.M. Kocur, A.I. Chowdhury, N. Sakulchaicharoen, H.K. Boparai, K.P. Weber, P. Sharma, M.M. Krol, L.M. Austrins, C. Peace, B.E. Sleep, D.M. O'Carroll, Environ. Sci.Technol., (2014) DOI: 10.1021/es4044209. .

[29] M.M. Krol, A.J. Oleniuk, C.M. Kocur, B.E. Sleep, P. Bennett, X. Zhong, D.M. O'Carroll, Environ. Sci.Technol., (2013).

[30] H.I. Gomes, C. Dias-Ferreira, A.B. Ribeiro, S. Pamukcu, Water Air Soil Poll., 224 (2013) 1-12.

[31] H.I. Gomes, C. Dias-Ferreira, A.B. Ribeiro, S. Pamukcu, Chemosphere, 99 (2014) 171-179.

[32] S. Pamukcu, L. Hannum, J.K. Wittle, J. Environ. Sci. Health A, 43 (2008) 934-944.

[33] E.H. Jones, D.A. Reynolds, A.L. Wood, D.G. Thomas, Ground Water, 49 (2010) 172-183.

[34] E. Rosales, J.P.G. Loch, C. Dias-Ferreira, Electrochim. Acta, 127 (2014) 27-33.

[35] Y.B. Acar, A.N. Alshawabkeh, Environ. Sci. Technol., 27 (1993) 2638-2647.

[36] G.C.C. Yang, C.H. Hung, H.C. Tu, J. Environ. Sci. HealthA, 43 (2008) 945-951.

[37] A.I.A. Chowdhury, D.M. O'Carroll, Y. Xu, B.E. Sleep, Adv. Water Resour., 40 (2012) 71-82.

[38] D.J. Wilson, J.M. Rodríguez-Maroto, C. Gómez-Lahoz, Sep. Sci. Technol., 30 (1995) 2937-2961.

[39] D.J. Wilson, J.M. Rodríguez-Maroto, C. Gómez-Lahoz, Sep. Sci.Technol., 30 (1995) 3111-3128.

[40] A.B. Ribeiro, E.P. Mateus, J.M. Rodríguez-Maroto, Sep.Purif. Technol., 79 (2011) 193-203.

[41] A.B. Ribeiro, J.M. Rodríguez-Maroto, E.P. Mateus, H. Gomes, Chemosphere, 59 (2005) 1229-1239.

[42] A.T. Lima, A.B. Ribeiro, J.M. Rodríguez-Maroto, E.P. Mateus, A.M. Castro, L.M. Ottosen, J. App. Electrochem., 40 (2010) 1689-1697.

[43] J.M. Paz-García, B. Johannesson, L.M. Ottosen, A.B. Ribeiro, J.M. Rodríguez-Maroto, Electrochim. Acta, 89 (2013) 436-444.

[44] J. Newman, Electrochemical Systems, Prentice Hall, Englewood Cliffs, 1991.

[45] J.K. Mitchell, Fundamentals of Soil Behavior, 2nd ed. ed., John Wiley & Sons, New York, 1993.

[46] R. Chang, J. Overby, General Chemistry – The Essential Concepts, McGraw-Hill, New York, 2011.

[47] K.R. Reddy, K. Darko-Kagy, C. Cameselle, Sep. Purif.Technol., 79 (2011) 230-237.

Table 1. Parameters used in modeling to simulate the experimental tests

Solid layer length, L: 20 cm
Solid layer Area, A: 10 cm^2 or 4 cm^2
Number of volume elements used to represented solid column, N: 20
Electrode compartment volume, V_0 and V_{N+1}: 650 cm^3
Faradaic efficiency $\eta = 1$
Δt: 5 seconds
Initial mass of nZVI injected in the system: 0.008 g (2 mL of 4 g L^{-1} solution)
Electric Potential: 5 V (Experiments 5 to 11) and 10 V (Experiment 12)

Diffusion control tests						
Test number	**Layer thickness (mm)**	**Matrix**	**Porosity**	**Electrolyte**	$D^*_{nZVI}\left(cm^2 s^{-1}\right)$	$U^*_{nZVI}\left(cm^2 V^{-1} s^{-1}\right)$
1	5	100% Kaolin	0.65	NaCl (0.001M)	$5.9\ 10^{-5}$	$-1.7\ 10^{-4}$
2	2	50% glass beads and 50% kaolin	0.57	NaCl (0.001M)	$4.6\ 10^{-5}$	$-1.5\ 10^{-4}$
3	2	75% glass beads and 25% kaolin	0.35	NaCl (0.001M)	$3.9\ 10^{-5}$	$-0.9\ 10^{-4}$
4	2	100% glass beads	0.20	NaCl (0.001M)	$1.8\ 10^{-5}$	$-0.5\ 10^{-4}$
Enhanced transport tests						
Test number	**Layer thickness (mm)**	**Matrix**	**Porosity**	**Electrolyte**	$D^*_{nZVI}\left(cm^2 s^{-1}\right)$	$U^*_{nZVI}\left(cm^2 V^{-1} s^{-1}\right)$
5	5	100% Kaolin	0.65	NaCl (0.001M)	$1.6\ 10^{-5}$	$-1.1\ 10^{-4}$
6	2	50% glass beads and 50 % kaolin	0.57	NaCl (0.001M)	$2.8\ 10^{-5}$	$2.4\ 10^{-5}$
7	2	75% glass beads and 25% kaolin	0.35	NaCl (0.001M)	$1.4\ 10^{-5}$	$2.1\ 10^{-6}$
8	2	100% glass beads	0.20	NaCl (0.001M)	$4.6\ 10^{-6}$	$8\ 10^{-6}$
9	5	100% Kaolin	0.65	NaOH (0.001M)	$1.7\ 10^{-5}$	$4.7\ 10^{-5}$
10	5	100% Kaolin	0.65	$CaCl_2$ (0.05M)	$4.8\ 10^{5}$	$-9.7\ 10^{7}$
11	5	100% Kaolin	0.65	Na_2SO_3 (0.1M)	$3.3\ 10^{-5}$	$1.8\ 10^{-4}$
12	5	100% Kaolin	0.65	NaCl (0.001M)	$2.3\ 10^{-5}$	$-5.7\ 10^{-5}$

Table 2. Distance covered by the iron nanoparticles in 2 d, 100% kaolin and 0.25 V cm^{-1}.

Electrolyte		Distance (m)
NaCl	0.001 M	0.29
NaOH	0.001 M	0.10
$CaCl_2$	0.05 M	0.16
Na_2SO_3	0.1 M	0.14

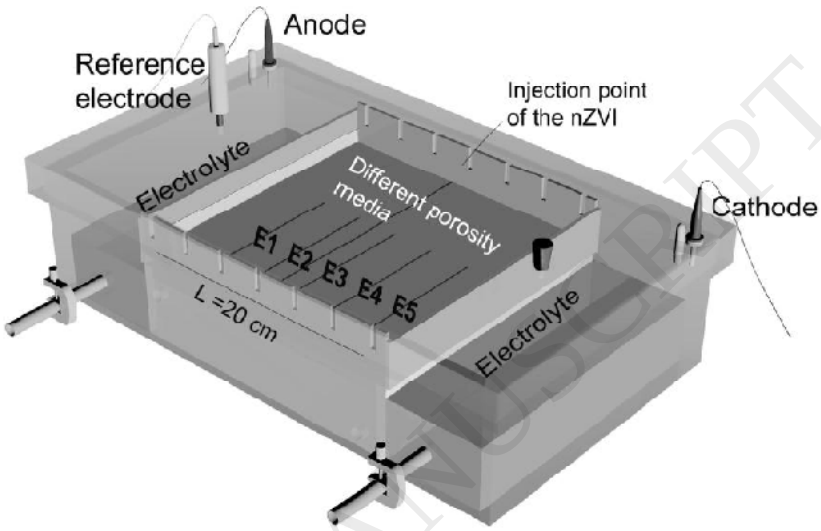

Figure 1. Modified electrophoretic cell used in the experiments [30, 31]. E1 to E5 are auxiliary platinum electrodes and represent the locations of the solid samples for iron quantification.

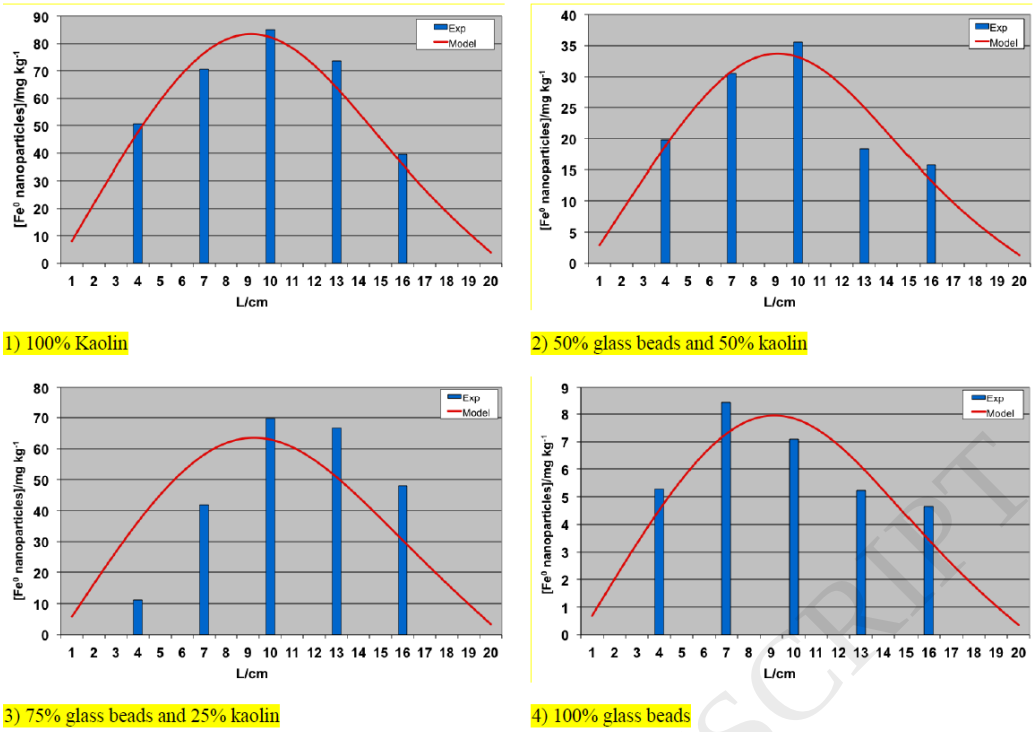

Figure 2. Iron concentrations across the electrophoretic cell in the diffusion control tests for the porous media tested (Experiments 1 to 4).

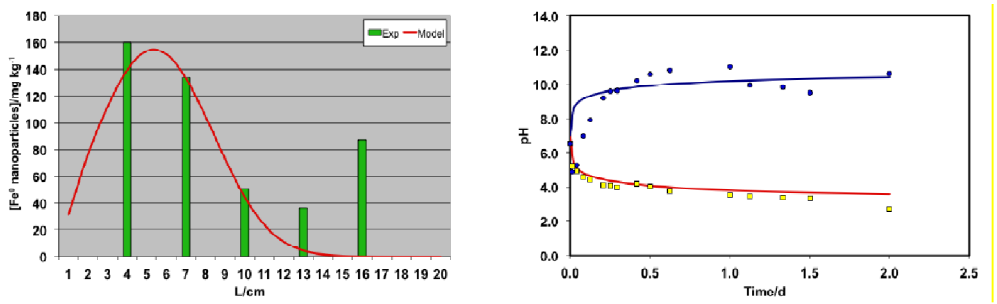

Exp. 5 a) 100% Kaolin

Exp. 5 b) 100% Kaolin

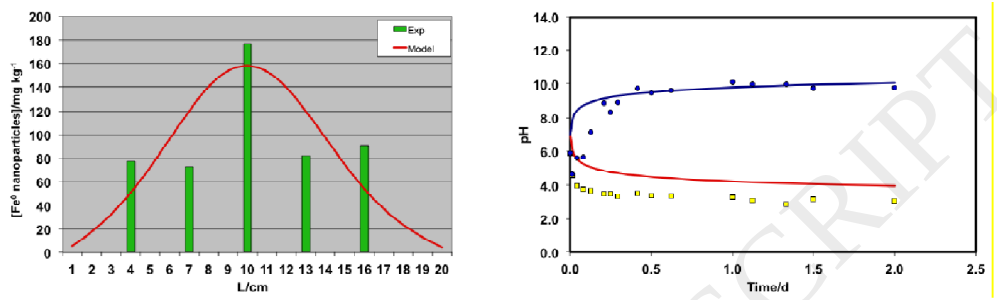

Exp. 6 a) 50% glass beads and 50 % kaolin

Exp. 6 b) 50% glass beads and 50 % kaolin

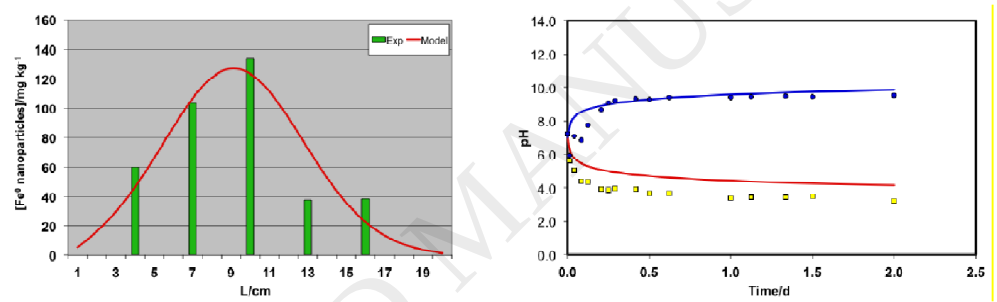

Exp. 7 a) 75% glass beads and 25% kaolin

Exp. 7 b) 75% glass beads and 25% kaolin

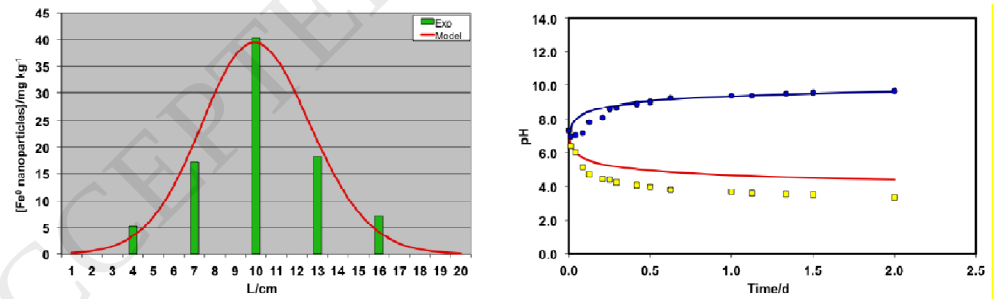

Exp. 8 a) 100% glass beads

Exp. 8 b) 100% glass beads

Figure 3. Enhanced transport tests: a) iron concentrations in the solid matrix and b) pH variation in the anolyte (yellow squares and red line) and catholyte (blue circles and line).

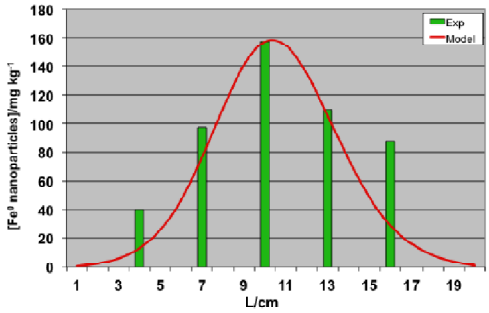

Exp. 9 a) 100% kaolin, NaOH (0.001 M)

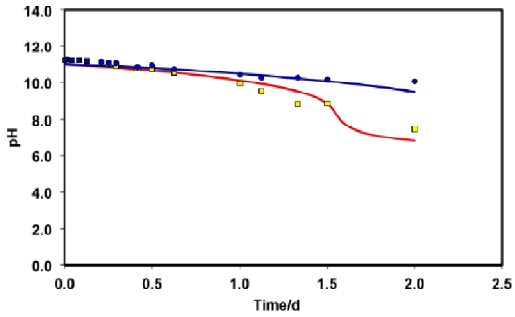

Exp. 9 b) 100% kaolin, NaOH (0.001 M)

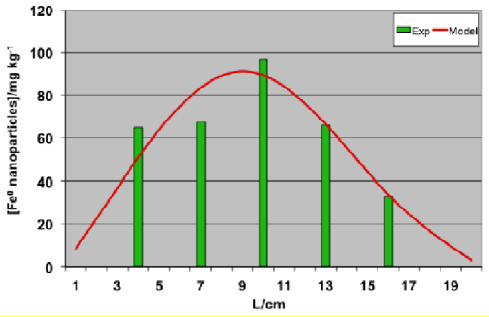

Exp. 10 a) 100% kaolin, $CaCl_2$ (0.05 M)

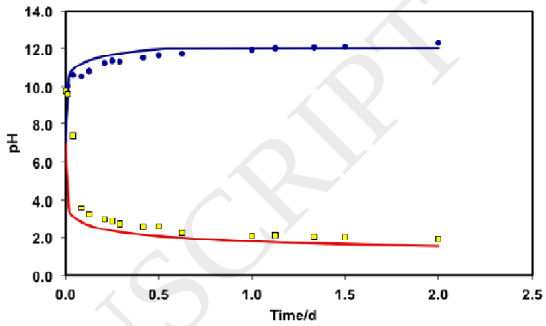

Exp. 10 b) 100% kaolin, $CaCl_2$ (0.05 M)

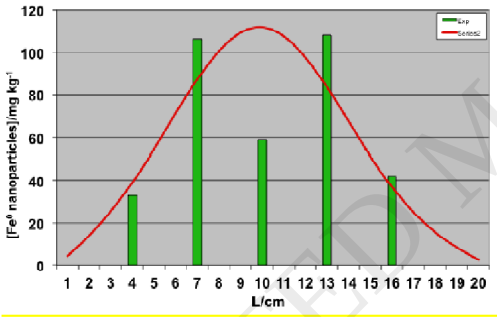

Exp. 11 a) 100% kaolin, Na_2SO_3 (0.1 M)

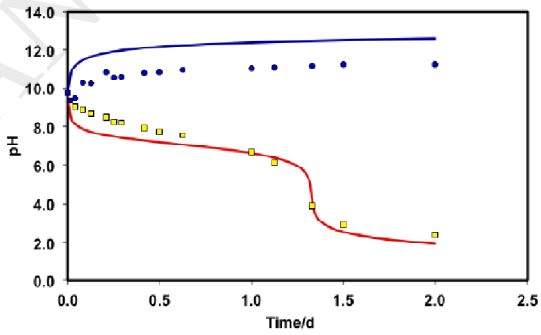

Exp. 11 b) 100% kaolin, Na_2SO_3 (0.1 M)

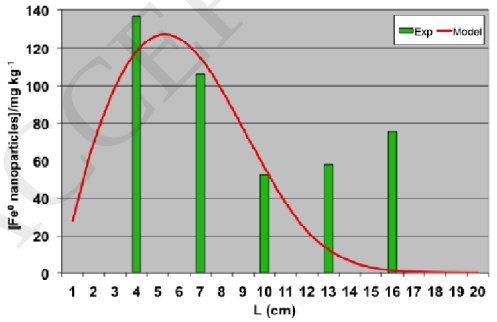

Exp. 12 a) 100% kaolin, NaCl (0.001 M)

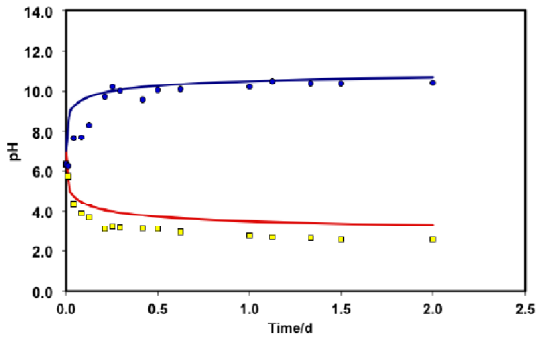

Exp. 12 b) 100% kaolin, NaCl (0.001 M)

Figure 4. Enhanced transport tests: a) iron concentrations in the solid matrix and b) pH variation in the anolyte (yellow squares and red line) and catholyte (blue circles and line).

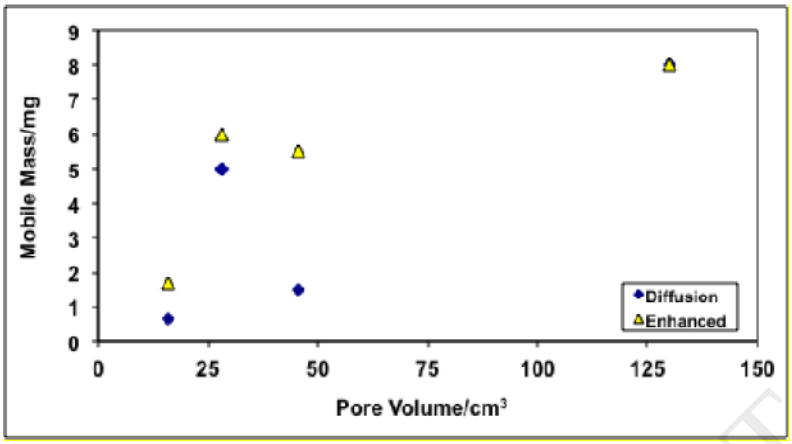

Figure 5. Mobile mass of nZVI in the diffusion and enhanced transport experiments.

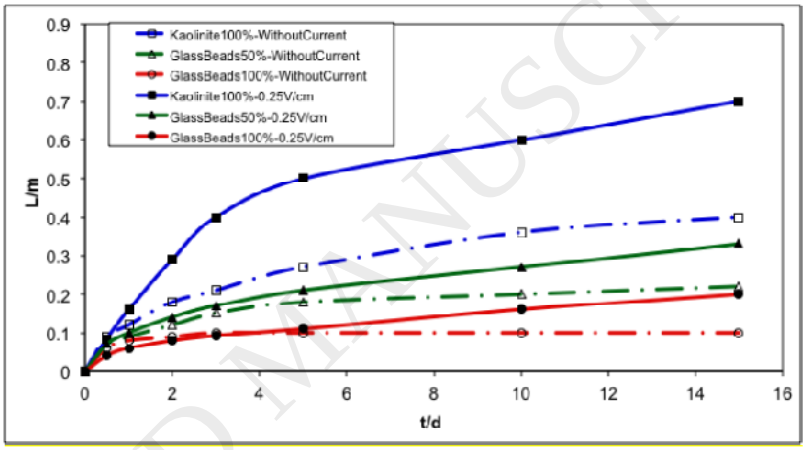

Figure 6. Prediction of the distances covered by nanoparticles in the different porosity media with and without current.